Power Feasible Region Ensuring Transient Stability of Droop-Based Multiconverters DC System

Xueshen Zhao, *Student Member, IEEE*, Li Guo, *Member, IEEE*, Lin Zhu, *Member, IEEE*, Xialin Li, *Member, IEEE*, Zhi Wang, and Chengshan Wang, *Senior Member, IEEE*

***Abstract*—This article systematically focuses on the transient stability problem of droop-based multiconverters dc (MCdc) system caused by large power disturbances. Therefore, a new and effective transient stability analysis method is proposed. In the present method, it starts with reduced-order nonlinear mathematical modeling, followed by Lyapunov energy function building, and then the inscription of the largest estimated domain of attraction (LEDA) and the power feasible region (PFR). First, a state-variable equivalent transformation method is proposed. With this method, the droop-based MCdc system can be modeled as an equivalent single-converter (ESC) model without ignoring any coupling effects between the control state-variables. Second, a Takagi–Sugeno fuzzy model of the ESC is developed, which is able to construct the LEDA. Third, to ensure the transient stability of the MCdc system under large power disturbance, the concept of PFR is proposed. Furthermore, a PFR inscription algorithm is given based on the LEDA. In addition, the influence of control parameters on the PFR is analyzed, which will provide guidelines for the optimization of the PFR. Finally, the time domain experiments are carried out on the RT-BOX hardware-in-the-loop experimental platform to verify the effectiveness of the above theoretical analysis.**

***Index Terms*—Equivalent single-converter (ESC) model, multiconverters dc (MCdc) system, PFR (PFR), transient stability analysis, Takagi–Sugeno (TS) fuzzy model.**

I. Introduction

With the increasing global warning caused by fossil energy generation, renewable energy generation (REG) is now being vigorously developed by countries around the world. The advantage of dc systems is that it can consume a high percentage of REGs and constant power loads (CPLs). This is the main reason why dc system is widely concerned by academic and industrial researchers [1]. The operating conditions of a multiconverters dc (MCdc) system are variable, which is mainly due to the output power (or input power) variations of REGs (or CPLs) [2]. From the perspective of transient stability of MCdc system, the above feasible power disturbance conditions should be selected accurately. Therefore, it is urgent to establish the transient stability analysis model of the MCdc system and construct its power feasible region (PFR).

In fact, the stability analysis of dc systems can be divided into small signal stability analysis and transient stability analysis (or large signal stability analysis) [2], [3]. The models used for small signal analysis are linearized models, such as state space matrices [4], [5], input/output impedances [6], [8], transfer functions [9], [10], [11], etc. Usually, these linearized models can be obtained by linearizing the nonlinear system around a certain operating point. And, it is difficult to know the effective range of linearization [12]. Therefore, the transient stability of the dc system after large power disturbances is difficult to be accurately evaluated by small signal methods. In fact, nonlinear mathematical models without linearization are suitable for transient stability studied [13], [14], [15]. In addition, the Lyapunov-based mathematical methods are the commonly used nonlinear mathematical tools [16]. With the Lyapunov-based mathematical method, the largest estimated domain of attraction (LEDA) of dc system can be constructed. The corresponding feasible power disturbances that can be tolerated by the dc system at a certain operating point will be given. Of course, it is usually conservative. The time domain results will confirm the validity of the feasible power perturbation obtained by the Lyapunov-based mathematical method. For dc systems with different control methods and topologies, the corresponding Lyapunov functions are also different [17], [18], [19], [20], [21]. In view of the single converter scenario, the Lyapunov functions of single-loop control and double-loop control are established by [18] and [19], respectively. The Lyapunov function of a cascaded system is constructed by using the modified mixed potential theory in [21]. However, the transient analysis studies in [17], [18], [19], [20], and [21] are mostly focused on single converter or simple cascaded systems. With the increase of the number of converters, the transient stability analysis of MCdc system will become more complex [21].

As pointed out in [22], the transient stability analysis of the MCdc system has been plagued by its high-order nonlinear coupled differential equations. To solve this problem, a nonlinear decoupling method is proposed in [22]. With this method, a high-order MCdc system can be decoupled into multiple first-order and second-order quadratic subsystems. Thus, the transient stability of the original high-order system can be indirectly

Manuscript received 6 August 2022; revised 20 October 2022; accepted 7 November 2022. Date of publication 15 November 2022; date of current version 14 February 2023. This work was supported in part by the National Key Research and Development Program of China under Grant 2020YFB1506800, in part by the China Postdoctoral Science Foundation under Project 2021M692378, and in part by the National Nature Science Foundation of China under Project 51977142. Recommended for publication by Associate Editor G. Oriti. *(Corresponding authors: Lin Zhu; Xialin Li.)*

The authors are with the Key Laboratory of Smart Grid of Ministry of Education, Tianjin University, Tianjin 300072, China (e-mail: zxs_1019@tju.edu.cn; liguo@tju.edu.cn; lin_zhu@tju.edu.cn; xialinlee@tju.edu.cn; 2020234352@tju.edu.cn; cswang@tju.edu.cn).

Color versions of one or more figures in this article are available at https://doi.org/10.1109/TPEL.2022.3222214.

Digital Object Identifier 10.1109/TPEL.2022.3222214

inferred from the transient stability results of these low-order subsystems. However, the strong coupling between state-variables is difficult to understand clearly. In addition, the effect of the strong coupling on the system transient stability will not be evaluated directly [23]. Therefore, it is necessary to construct the reduced-order nonlinear mathematical model by considering the coupling [24]. In [25], a second-order nonlinear model considering the coupling between the filter circuits of the MCdc system was established. Based on the simplified differential equations of [25], the Lyapunov function was constructed by [26]. From the system-level point of view, an equivalent nonlinear model of droop-controlled dc microgrid was established [27], [28]. However, the validity of the above transient stability analysis needs to be further verified. This is mainly due to the neglect of voltage control parameters which have an important impact on the transient stability of the system. It is widely accepted that double-loop control is better than single-loop control [13]. This is because the main purpose of the current inner loop control is to stabilize the dc system [29]. The voltage outer loop, on the other hand, provides the reference signal for the current inner loop [30]. For droop-based MCdc systems (including voltage and current double-loop control), the interaction mechanism between converters is not clear. This is the main reason why the reduced-order nonlinear model of the droop-based MCdc system has not been reported.

Assumed the reduced-order nonlinear model of the droop-based MCdc system can be established, it will be easy to construct a Lyapunov function of the reduced-order nonlinear model. However, it should be noted that the LEDA portrayed by the Lyapunov function has limitations. The LEDA of the MCdc system can be inscribed by using the Lyapunov function at a postoperating point. In the actual operation of the MCdc system, a number of large power perturbations will occur. The postoperating point also changes after each power disturbance. Then, the LEDA will need to be reconstructed. This is time-consuming and laborious. From this point of view, the concept of PFR will be more feasible and practical. To the authors' best knowledge, this concept has not been proposed yet. The advantage of the PFR is that it contains a lot of transient stability/instability information. That is, the transient stability of many large power disturbances can all be evaluated by the same PFR. For example, if the above power disturbances are outside the feasible region, then the MCdc system will lose its transient stability. Conversely, the transient stability of the MCdc system can be guaranteed. Therefore, the PFR is very useful in ensuring transient stable operation under large power disturbances. However, how to depict the PFR of droop-based MCdc system is still an unsolved problem.

In addition, how to enhance the transient stability of the system has always been a very hot research topic. Especially for dc system, which is controlled by the classical single-loop or double-loop proportional–integral (PI) controller. As we all know, unreasonable control parameters are the root cause of system transient instability [14], [15]. Fundamentally speaking, the transient stability of the system can be guaranteed by reasonable control parameters. For the transient instability problem of the dc system, three solutions are introduced [28], [30]. The first solution is to replace the PI controller with a nonlinear controller. A nonlinear control method is introduced in [30], which can estimate the uncertain large disturbance of CPL power. To deal with the voltage transient instability caused by system uncertainty, a predictive control method is reported in [31]. In the research work on nonlinear control, the transient stability of the system is proved by mathematical derivation. And, the specific values of the control parameters are not considered in this derivation procedure. Then, from a theoretical point of view, the nonlinear control parameters are difficult to be designed. In order to design appropriate control parameters, a large number of time-domain simulation/experimental results are often required. It will take a lot of time and effort. Keeping the PI controller and control parameters unchanged, the second solution adds some new controllers to the system [19]. In order to compensate the system nonlinearity introduced by CPL, a nonlinear state-feedback control method is presented by [25]. However, this method needs to measure the input current of all CPLs. Moreover, the real time and accuracy of data transmission are strictly required. However, compared with the widely used PI controller, the versatility of these new controllers needs to be further verified. The third solution is to optimize the PI control parameters. In literature [28], it is observed that the effect of virtual resistor on transient stability is opposite to that of voltage deviation. Thus, a virtual resistor tradeoff design method is proposed. Compared with the virtual resistor, the control parameters do not need to be compromised. But, the influence of voltage control parameters on transient stability has not been reported. With the help of the mixed potential theory, the influence of voltage control parameters on transient stability boundary is evaluated by [21]. However, in literature [21], the research object is the cascaded system rather than the MCdc system. To sum up, from the perspective of PFR of the droop-based MCdc system, the design guideline of double-loop control parameters has not been reported.

For the above unresolved transient stability problem, a new and effective transient stability analysis method is proposed in this article. The method contains the establishment of the equivalent single-converter model and its Takagi–Sugeno (TS) fuzzy model, as well as the inscription of the largest estimated attraction domain and the PFR. The main contributions can be drawn as follows.

1) To simplify the high-order mathematical model of droop-based multiconverters dc (MCdc) system, a state-variable equivalent transformation method is proposed. With this method, multiple current control state-variables in the system can be directly equated to one current control state-variable. Similarly, the equivalence of voltage control state-variables is also feasible. Then, the equivalent single-converter (ESC) model of the MCdc system is developed in this way. Because almost any coupling effect between state-variables is considered, the MCdc system and its ESC model necessarily have consistent stability. Based on the sixth-order nonlinear differential equations of the ESC, the corresponding TS fuzzy model is

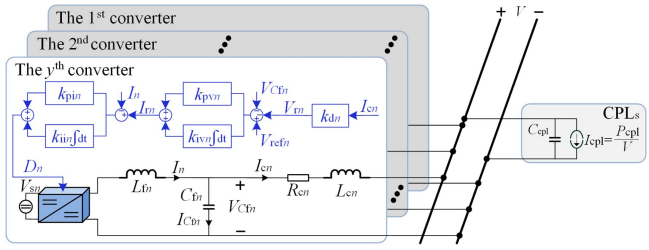

Fig. 1 Topology of a typical single-bus MCdc system.

developed. Moreover, the LEDA can be constructed by using the TS fuzzy model. This LEDA is feasible for ensuring the transient stability of both the MCdc system and its ESC model.

2) To ensure the transient stability of droop-based MCdc systems, the concept of PFR is proposed for the first time. Then with the obtained LEDA, a PFR construction algorithm is proposed to obtain the feasible region. In addition, the effects of current, voltage, and droop control parameters on the PFR are systematically investigated.

The rest of this article is organized as follows. The transient stability problem of the MCdc system caused by large power disturbances is introduced in Section II. In Section III, the ESC model of the MCdc system is established by the proposed state-variable equivalent transformation method. With the help of the LEDA inscribed by the TS fuzzy model, the PFR and its construction algorithm are presented in Section IV. The effect of the control parameters on the PFR is discussed in Section V. Section VI concludes this article.

II. Transient Instability Issue of the Studied MCDC System

The topology of a typical single-bus MCdc system (including n converters) studied in this article is shown in Fig. 1. The topology and filter parameters design guidelines of the dc–dc converter used in this article are recommended by [25] and [26].

As shown in Fig. 1, the droop-based double-loop controller is considered by each converter. And these converters are connected to the common single-bus MCdc system through cables. For the transient instability issue of MCdc system, the switch model of a typical system is built in the RT-BOX hardware-in-the-loop experimental platform, as shown in Fig. 2. Without losing generality, the circuit parameters or control parameters of each converter studied in this article are different, as shown in Tables II and III, respectively. In Table I, six disturbance cases of CPL are given. For the above two group of control parameters, the MCdc system is small signal stable at the corresponding operating points (the power of CPL is 12, 14, 15.5, and 17 MW, respectively). The corresponding small signal theory analysis results are provided by Figs. 25 and 26. However, small signal stability is a necessary nonsufficient condition for transient stability (or large signal stability). Therefore, with the power step of CPL, transient stability problem will occur. The details of the experimental results (ERs) are shown in Fig. 3.

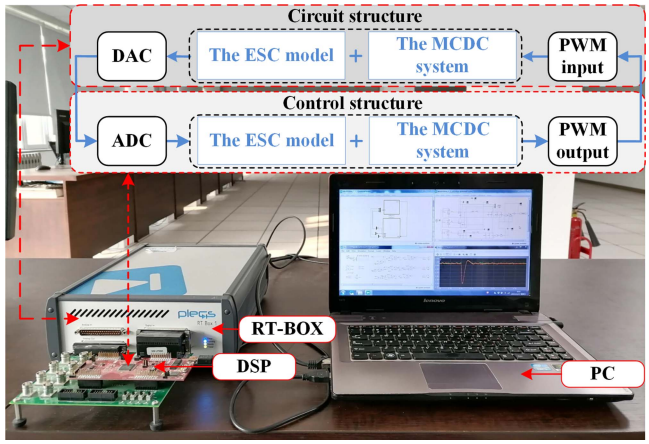

Fig. 2. RT-BOX hardware-in-the-loop experimental platform.

TABLE I
Case Setting for the MCDC System

Control parameters	Number	Power variation of CPL	Transient stability
The first group	Case 1	From 12 to 14 MW	Stable
	Case 2	From 14 to 15.5 MW	Stable
	Case 3	From 12 to 15.5 MW	Unstable
The second group	Case 4	From 12 to 15.5 MW	Stable
	Case 5	From 15.5 to 17 MW	Stable
	Case 6	From 12 to 17 MW	Unstable

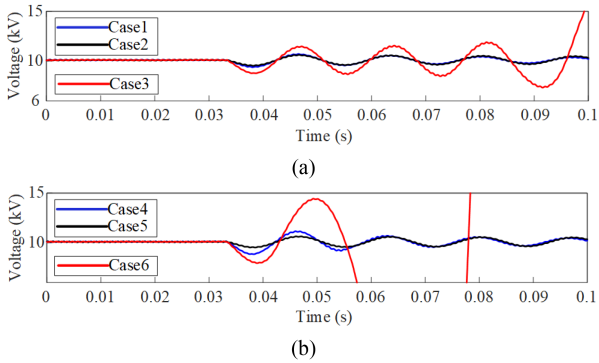

Fig. 3. Experimental results of the MCdc system. (a) First group control parameters. (b) Second group control parameters.

The experimental results of the MCdc system under the first group control parameters are shown in Fig. 3(a). For two closer operating points (e.g., Case 1 from 12 to 14 MW, or Case 2 from 14 to 15.5 MW), the transient processes of the MCdc system is stable. However, when the CPL power steps from 12 to 15.5 MW, the experimental results of dc bus voltage become unstable.

At the second group of control parameters, the dc bus voltage can be stabilized after the CPL step from 12 to 15.5 MW. And as the CPL step from 12 to 17 MW, the MCdc system lose the transient stability, as shown in Fig. 3(b).

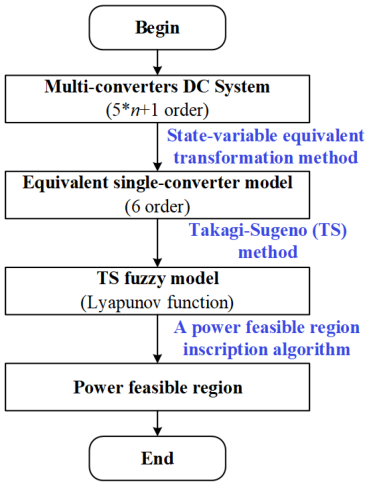

Fig. 4. Transient stability analysis procedure for multiconverters DC system.

Based on the above experimental results, it can be known that the transient instability of MCdc system may occur in large power disturbance scenarios. Moreover, the transient stability of the MCdc system can be improved by changing the control parameters. However, the high-order nonlinear coupled differential equations of the MCdc system bring great difficulties to its transient stability analysis. In order to reduce the computational burden of transient stability analysis of MCdc systems, a lot of innovative work has been carried out, such as nonlinear decoupling or coupling equivalence modeling [22], [23], [24], [25], [26], [27]. But, the methods of [22], [23], [24], [25], [26], and [27] have the following drawbacks, such as indirectly considering the coupling or neglecting some of the control parameters, etc.

If an equivalent nonlinear model of the MCdc system is developed, then its LEDA will be subsequently portrayed. Suppose, there are two operating points in the MCdc system, one is the predisturbance operating point and the other is the postdisturbance operating point. Then, the LEDA of the equivalent nonlinear model at the postdisturbance operating point can be constructed [17], [18], [19], [20], [21]. If the predisturbance operating point is within or on the boundary of the LEDA of the postdisturbance operating point, the MCdc system will be transient stable. On the contrary, transient instability may occur. However, as the postdisturbance operating point changes, the LEDA will need to be reconstructed. Compared to LEDA, the PFR will contain more transient stability information. To the best of the authors' knowledge, the concept of PFR and its construction algorithm have not been proposed yet. Moreover, the influence of the control parameters on this PFR is worth evaluating. In summary, the detailed procedure of the transient stability analysis method proposed in this article is shown in Fig. 4.

III. ESC Model of the MCdc System

In this section, a state-variable equivalent transformation method is proposed. With the help of this method, the ESC model of the MCdc system will be developed. Almost all details of the MCdc system are taken into account by the ESC model, so that they have consistent transient stability. Most critically, the ESC model has the advantage of lower computational complexity.

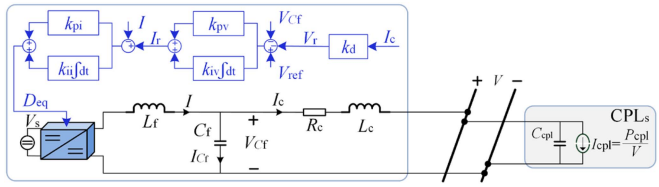

Fig. 5. Topology of the ESC model.

A. Equivalent Transformation of Voltage Control State-Variables

The topology of the ESC model of the studied MCdc system is shown in Fig. 5. The topology and filter parameters design guidelines of the dc–dc converter used in this article are recommended by [25].

Due to the different coupling mechanisms, the equivalent transformation processes of voltage and current state-variables will be introduced, respectively. Considering the input–output relationship of the control signal, the equivalent transformation of voltage control state-variables will be described in detail first.

The control parameters of each converter in this article are designed according to the design guidelines recommended by [31]. Then, the relationship between the control parameters of each converter can be expressed as (B.1) and (B.2), respectively. With the help of this guideline, the dynamic characteristics of each converter are consistent. And, the voltage control loops (including droop control) of each converter and the ESC model can be written as

$$\sum_{y=1}^{n}(I_{\mathrm{r}y}) = \sum_{y=1}^{n}\begin{pmatrix} k_{\mathrm{pv}y}\left(V_{\mathrm{ref}y} - I_{\mathrm{c}y}\cdot k_{\mathrm{d}y} - V_{\mathrm{Cf}y}\right) \\ +k_{\mathrm{iv}y}\int\left(V_{\mathrm{ref}y} - I_{\mathrm{c}y}\cdot k_{\mathrm{d}y} - V_{\mathrm{Cf}y}\right)dt \end{pmatrix} \tag{1}$$

$$I_{\mathrm{r}} = \begin{pmatrix} k_{\mathrm{pv}}\left(V_{\mathrm{ref}} - I_{\mathrm{c}}\cdot k_{\mathrm{d}} - V_{\mathrm{Cf}}\right) \\ +k_{\mathrm{iv}}\int\left(V_{\mathrm{ref}} - I_{\mathrm{c}}\cdot k_{\mathrm{d}} - V_{\mathrm{Cf}}\right)dt \end{pmatrix} \tag{2}$$

where $I_{\mathrm{r}y}$ and I_{r} are the filter inductor current reference of the yth converter ($y = 1,2,\ldots,n$) and the ESC model, respectively, $I_{\mathrm{c}y}$ and I_{c} are the output current of the yth converter ($y = 1,2,\ldots,n$) and the ESC model, respectively, $V_{\mathrm{ref}y}$ and V_{ref} are the voltage reference of the yth converter and the ESC model, respectively, $k_{\mathrm{d}y}$ and k_{d} are the droop coefficient of the yth converter and the ESC model, respectively, $V_{\mathrm{Cf}y}$ and V_{Cf} are the output voltage of the yth converter and the ESC model, respectively, $k_{\mathrm{pv}y}$ and $k_{\mathrm{iv}y}$ are the proportional and integral gains of the voltage controller $G_{\mathrm{vc}y}(s)$ of the yth converter, respectively, k_{pv} and k_{iv} are the proportional and integral gains of the voltage controller $G_{\mathrm{vc}}(s)$ of the ESC model, respectively, h_y is the load sharing coefficient ($\Sigma hy = 1$) of the yth converter.

If it is assumed that the MCdc system can be equivalent to an ESC model. Then, the output current I_{c} is considered to be the sum of each output current $I_{\mathrm{c}y}$

$$\begin{cases} I_{\mathrm{c}} = \sum_{y=1}^{n}(I_{\mathrm{c}y}) \\ I_{\mathrm{c}y} = I_{\mathrm{c}}\cdot h_y. \end{cases} \tag{3}$$

Combining (1) to (2), the equivalent analytical equations for the voltage control state-variables can be established as follows:

$$k_{\mathrm{pv}}\left(V_{\mathrm{ref}}-I_{\mathrm{c}}\cdot k_{\mathrm{d}}-V_{Cf}\right)=\sum_{y=1}^{n}\left\{k_{\mathrm{pv}y}\left(V_{\mathrm{ref}y}-I_{cy}\cdot k_{\mathrm{d}y}-V_{Cfy}\right)\right\} \tag{4}$$

$$k_{\mathrm{iv}}\int\left(V_{\mathrm{ref}}-I_{\mathrm{c}}\cdot k_{\mathrm{d}}-V_{Cf}\right)dt=\sum_{y=1}^{n}\left\{k_{\mathrm{iv}y}\int\left(V_{\mathrm{ref}y}-I_{cy}\cdot k_{\mathrm{d}y}-V_{Cfy}\right)dt\right\} \tag{5}$$

where $\int(V_{\mathrm{ref}y}\text{-}I_{\mathrm{c}y}k_{\mathrm{d}y}\text{-}V_{Cfy})\mathrm{d}t$ and $\int(V_{\mathrm{ref}}\text{-}I_{\mathrm{c}}k_{\mathrm{d}}\text{-}V_{Cf})\mathrm{d}t$ are the voltage control state-variables of the yth converter and the ESC model, respectively. The multiple parallel transmission lines in Fig. 1 can be equated to one [24]. And, the relationship between the output voltage of each converter and the ESC model can be given as follows:

$$V_{Cf}\approx V_{Cf1}\approx\ldots\approx V_{Cfy}. \tag{6}$$

Substituting (6) into (5) and considering (B.1) and (B.3) in Appendix B, it can be deduced that $\int(V_{\mathrm{ref}y}\text{-}I_{\mathrm{c}y}k_{\mathrm{d}y}\text{-}V_{Cfy})\mathrm{d}t$ is approximately equal to $\int(V_{\mathrm{ref}}\text{-}I_{\mathrm{c}}k_{\mathrm{d}}\text{-}V_{Cf})\mathrm{d}t$, as

$$\int\left(V_{\mathrm{ref}}-I_{\mathrm{c}}\cdot k_{\mathrm{d}}-V_{Cf}\right)dt\approx\int\left(V_{\mathrm{ref}y}-I_{cy}\cdot k_{\mathrm{d}y}-V_{Cfy}\right)dt. \tag{7}$$

Then, the analytical equations of the voltage control parameters between the yth converter and the ESC model can be obtained

$$\begin{cases}k_{\mathrm{pv}}\approx\sum_{y=1}^{n}\left(k_{\mathrm{pv}y}\right)\\ k_{\mathrm{iv}}\approx\sum_{y=1}^{n}\left(k_{\mathrm{iv}y}\right).\end{cases} \tag{8}$$

B. Equivalent Transformation of Current Control State-Variables

As can be seen from Figs. 1, 3, 4, and 5, the relationship of the filter inductor currents between the yth converter and the ESC model can be written as

$$\frac{dI}{dt}=\sum_{y=1}^{n}\left(\frac{dI_y}{dt}\right) \tag{9}$$

where I_y and I are the filter inductor current of the yth converter and the ESC model, respectively.

Further, considering the duty signal, (9) can be reformulated as follows:

$$\frac{D_{\mathrm{eq}}\cdot V_{\mathrm{s}}-V_{Cf}}{L_{\mathrm{f}}}\approx\sum_{y=1}^{n}\left(\frac{D_y\cdot V_{\mathrm{s}y}-V_{Cfy}}{L_{\mathrm{f}y}}\right) \tag{10}$$

where D_k and D_{eq} are the duty of the yth converter and the ESC model, respectively.

Based on the derivation process and the assumptions of current control parameters in Appendix B, (11) can be obtained as

$$\begin{cases}\frac{k_{\mathrm{pi}}}{L_{\mathrm{f}}}\left(I_{\mathrm{r}}-I\right)\approx\sum_{y=1}^{n}\left(\frac{k_{\mathrm{pi}y}}{L_{\mathrm{f}y}}\left(I_{\mathrm{r}y}-I_y\right)\right)\\ \frac{k_{\mathrm{ii}}}{L_{\mathrm{f}}}\int\left(I_{\mathrm{r}}-I\right)dt\approx\sum_{y=1}^{n}\left(\frac{k_{\mathrm{ii}y}}{L_{\mathrm{f}y}}\int\left(I_{\mathrm{r}y}-I_y\right)dt\right)\end{cases} \tag{11}$$

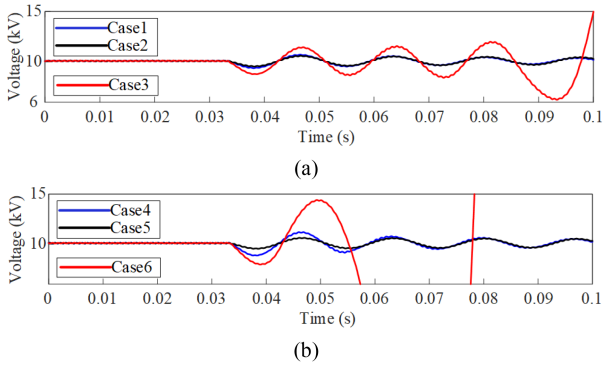

Fig. 6. Experimental results of the ESC. (a) First group of control parameters. (b) Second group of control parameters.

where $\int(I_{\mathrm{r}y}\text{-}I_y)\mathrm{d}t$ and $\int(I_{\mathrm{r}}\text{-}I)\mathrm{d}t$ are the current control state-variables of the yth converter and the ESC model, respectively. Then, the analytical equation between $\int(I_{\mathrm{r}y}\text{-}I_y)\mathrm{d}t$ and $\int(I_{\mathrm{r}}\text{-}I)\mathrm{d}t$ is shown in (11). The analytical equations of the current control parameters between the yth converter and the ESC model can be given as follows:

$$\begin{cases}k_{\mathrm{pi}}\approx L_{\mathrm{f}}\sum_{y=1}^{n}\left(\frac{k_{\mathrm{pi}y}h_y}{L_{\mathrm{f}y}}\right)\\ k_{\mathrm{ii}}\approx L_{\mathrm{f}}\sum_{y=1}^{n}\left(\frac{k_{\mathrm{ii}y}h_y}{L_{\mathrm{f}y}}\right).\end{cases} \tag{12}$$

In summary, an MCdc system containing $5{*}n{+}1$ state-variables can be modeled as an ESC model, which is represented by six state-variables.

C. Validation of ESC Model

Based on the MCdc system shown in Tables II and III, the ESC model is also built on the RT-BOX hardware-in-the-loop experimental platform. Under the CPL disturbance shown in Table I, the dc bus voltage experimental results of the ESC model are shown in Fig. 6. According to the experimental results provided by Figs. 3 and 6, the dc bus voltages of both the MCdc system and its ESC model exhibit the same transient stability and instability. Then, the effectiveness of the proposed equivalent transformation method of state-variables is verified. In addition, the equivalent transformation verification results for voltage or current control state-variables are also given by this article, as shown in Fig. 27 to (B.6).

IV. Construction of Largest Estimated Domain of Attraction and PFR

In this section, the TS fuzzy model is established to portray the LEDA of the ESC model. Further, to ensure the transient stability of the ESC model, a concept of PFR is proposed in this article. With the help of the obtained LEDA, a simple algorithm is proposed to inscribe this PFR. Of course, the LEDA and PFR obtained based on the ESC model are also feasible for the MCdc system.

A. Constructing LEDA Based on TS Fuzzy Model

For the above transient stability problem of the ESC model, a nonlinear stability analysis tool is required to estimate the domain of attraction of the operating point. Because the circuit dynamics and control dynamics of the ESC model need to be considered simultaneously, the TS fuzzy model approach is widely used in transient stability analysis [2].

From Fig. 5, state equations of the ESC model can be expressed as (C.2) in Appendix C. Obviously, (C.2) can be written in the matrix form $\dot{\boldsymbol{x}} = \boldsymbol{A}(\boldsymbol{x})\boldsymbol{x}$, where $\boldsymbol{A}(\boldsymbol{x})$ is a nonlinear matrix function containing state-variables and $\boldsymbol{x} = [x_1\ x_2\ x_3\ x_4\ x_5\ x_6]^{\mathrm{T}}$. For convenience, $k_{\mathrm{ii}}\int(I_{\mathrm{r}}\text{-}I)\mathrm{d}t$ and $k_{\mathrm{iv}}\int(V_{\mathrm{ref}}\text{-}I_{\mathrm{c}}k_{\mathrm{d}}\text{-}V_{Cf})\mathrm{d}t$ are defined as S_{ii} and S_{iv}, respectively. Then, the state-variables x_1-x_6 are defined as follows:

$$\begin{cases} x_1 = S_{\mathrm{ii}} - S_{\mathrm{ii0}} & x_2 = I - I_0 & x_3 = S_{\mathrm{iv}} - S_{\mathrm{iv0}} \\ x_4 = V_{Cf} - V_{Cf0} & x_5 = I_{\mathrm{c}} - I_{\mathrm{c0}} & x_6 = V - V_0 \end{cases} \tag{13}$$

where the subscript "0" indicates the steady-state value. For convenience, (C.2) is moved from the equilibrium point [as shown in (14)] to the origin. Then, (C.3) is available.

$$\begin{cases} S_{\mathrm{ii0}} = \frac{V_{Cf0}}{V_{\mathrm{s}}} & I_0 = I_{\mathrm{c0}} & S_{\mathrm{iv0}} = I_{\mathrm{c0}} \\ V_{Cf0} = V - I_{\mathrm{c0}}k_{\mathrm{d}} & I_{\mathrm{c0}} = \frac{V - V_0}{k_{\mathrm{d}}} & V_0 = \frac{V}{2} + \sqrt{\frac{V^2}{4} - P_{\mathrm{cpl}}k_{\mathrm{d}}}. \end{cases} \tag{14}$$

For the ESC model, the only nonlinearity in its mathematical model (C.3) is $u(x_6) = 1/(x_6+V_0)$. Assuming $x_6 \in [x_{6\min}, x_{6\max}]$, the TS fuzzy model of (C.3) in the region $\psi = \{x \in \mathbf{R}^2 \mid x_{6\min} \le x_6 \le x_{6\max}\}$ can be described by the following two fuzzy rules.

Rule $\boldsymbol{R^1}$: If x_6 is closed to $x_{6\max}$, then set $u_{\min} = 1/(x_{6\max}+V_0)$.
Rule $\boldsymbol{R^2}$: If x_6 is closed to $x_{6\min}$, then set $u_{\max} = 1/(x_{6\min}+V_0)$.

The weighting functions ω_1 and ω_2 can be expressed as follows:

$$\begin{cases} \omega_1(x_6) = \frac{x_6 - x_{6\min}}{x_{6\max} - x_{6\min}} \\ \omega_2(x_6) = \frac{x_{6\max} - x_6}{x_{6\max} - x_{6\min}}. \end{cases} \tag{15}$$

Further, the TS fuzzy model of (C.3) in region ψ can be obtained as follows:

$$\dot{\boldsymbol{x}} = \boldsymbol{g}(\boldsymbol{x}) = \sum\nolimits_{i=1}^{2} \{\omega_i(x_6) A_i \boldsymbol{x}\}. \tag{16}$$

If the linear matrix inequality (17) is feasible, then $\Omega = \{\boldsymbol{x} \in \mathbf{R}^6 \mid \boldsymbol{x}^{\mathrm{T}}\boldsymbol{M}\boldsymbol{x} \le \min(x_1, x_2, x_3, x_4, x_5, x_{6\min})\}$ is a subset of the true domain of attraction of (C.3), i.e., the estimated domain of attraction

$$\begin{cases} M = M^T > 0 \\ A_1^T M + M A_1 < 0 \\ A_2^T M + M A_2 < 0 \end{cases} \tag{17}$$

where $\boldsymbol{M}$ is a symmetric matrix. Obviously, the smaller $x_{6\min}$ is, the larger Ω is. And, the boundary value of $x_{6\min}$ is denoted as $x_{6\min,\mathrm{c}}$. Subsequently, the Lyapunov function of the ESC model can be constructed as $V(\boldsymbol{x}) = \boldsymbol{x}^{\mathrm{T}}\boldsymbol{M}\boldsymbol{x}/\mathrm{c}$, where $\mathrm{c} = \min V(x_1, x_2, x_3, x_4, x_5, x_{6\min,\mathrm{c}})$. Then, the LEDA of the ESC model can be expressed as

$$\Omega_V = \{\boldsymbol{x} : V(\boldsymbol{x}) \le 1\}. \tag{18}$$

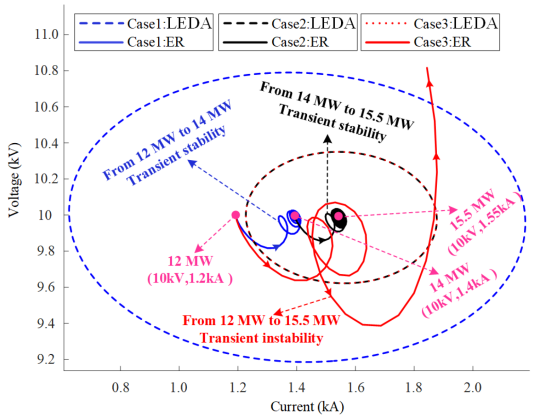

Fig. 7. LEDA from Cases 1 to 3.

After suffering a large power disturbance, the transient stability of the ESC model (or MCdc system) can be judged by the following criterion:

$$0 \le V(\boldsymbol{x_{e0}} - \boldsymbol{x_{e1}}) \le 1 \tag{19}$$

where $\boldsymbol{x_{e0}}$ and $\boldsymbol{x_{e1}}$ are the states of the ESC model before and after the large power disturbance, respectively. If (19) is feasible, then $\boldsymbol{x_{e0}}$ lies within or on the boundary of the LEDA of $\boldsymbol{x_{e1}}$. Then, the ESC model is transiently stable after suffering a large power disturbance. Conversely, it is difficult to evaluate the transient stability of the ESC model in theory. This is due to the inherent conservatism of Lyapunov's direct method.

B. Theoretical Explanation of the Above Transient Stability and Instability Issues Based on the LEDA

With (19), the LEDA of the ESC model will be constructed. In the first group control parameters, the three operating states ($\boldsymbol{x_{e,f1}}$, $\boldsymbol{x_{e,f2}}$, and $\boldsymbol{x_{e,f3}}$) of the MCdc system are given by the corresponding three operating points (12 MW, 14 MW and 15.5 MW for CPL). For Case 1, $V(\boldsymbol{x_{e,f2}}\text{-}\boldsymbol{x_{e,f1}}) = 0.2141 < 1$. Then, the 12-MW operating point lies within the LEDA of the 14-MW operating point. This provides the theoretical support for the transient stabilization experimental results (ERs) of the MCdc system and its ESC model in Case 1. Since the LEDA of (18) is in 6-D form, it cannot be presented directly in graphical form. Therefore, the state-variables of I and V are usually chosen to portray the LEDA in 2-D2 form, as shown in Fig. 7. Similarly, for Case 2, $V(\boldsymbol{x_{e,f3}}\text{-}\boldsymbol{x_{e,f2}}) = 0.4237 < 1$, which corresponds to the transient stability of the MCdc system and its ESC model. Unfortunately, in Case 3, $V(\boldsymbol{x_{e,f3}}\text{-}\boldsymbol{x_{e,f1}}) = 2.3059 > 1$, which means that the 12-MW operating point lies outside the LEDA of the 15.5-MW operating point. Then, for the MCdc system and its ESC model under the 12-MW operating point, a 3.5-MW CPL power disturbance will cause their transient instability.

The theoretical analysis results of the second group control parameters are shown in Fig. 8. And, the operating states for operating points of 12, 15.5, and 17 MW are $\boldsymbol{x_{e,s4}}$, $\boldsymbol{x_{e,s5}}$, and

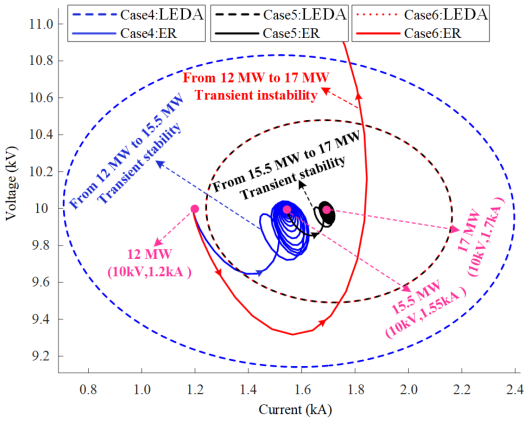

Fig. 8. LEDA from Cases 4 to 6.

$\boldsymbol{x}_{\mathbf{e,s6}}$, respectively. For Case 4, $V(\boldsymbol{x}_{\mathbf{e,s5}}\text{-}\boldsymbol{x}_{\mathbf{e,s4}}) = 0.6335 < 1$. This means that the $\boldsymbol{x}_{\mathbf{e,s4}}$ operating state is within the LEDA of the $\boldsymbol{x}_{\mathbf{e,s5}}$ operating state. And it can be inferred that the transient stability of MCdc system and its ESC model has been significantly improved with the help of the second group control parameters. In addition, $V(\boldsymbol{x}_{\mathbf{e,s6}}\text{-}\boldsymbol{x}_{\mathbf{e,s5}}) = 0.2731 < 1$, which provides the theoretical support for the stable experimental results of Case 5. For Case 6, $V(\boldsymbol{x}_{\mathbf{e,s6}}\text{-}\boldsymbol{x}_{\mathbf{e,s4}}) = 3.0324 > 1$. This is the theoretical explanation of the transient instability results.

As mentioned above, the validity of the LEDA is verified by the experimental results. From the perspective of the transient stability of the MCdc system during CPL disturbance, how to construct PFRs will be described in detail.

C. Power Feasible Region Construction Algorithm

1) *The Concept of PFR:* PFR is defined as: the feasible region of power to ensure the transient stability of the MCdc system during power disturbances. And it can be expressed as

$$\Omega_{\boldsymbol{P}} \triangleq \{P \in R \,|\, \boldsymbol{x}_{\mathbf{e0}} \in \Omega_V(\boldsymbol{x}_{\mathbf{e1}}), P_1 \le P_{\text{neq}}\} \tag{20}$$

where Ω_{P} is the defined PFR, $\Omega_V(\boldsymbol{x}_{\mathbf{e1}})$ is the LEDA of operating point P_1, P_{neq} is the permissible limiting value of the MCdc system according to its rated capacity. If the conditions in (20) are satisfied, then the MCdc system will be transient stable as it steps from $\boldsymbol{x}_{\mathbf{e0}}$ to $\boldsymbol{x}_{\mathbf{e1}}$.

2) *A PFR Construction Algorithm:* Given a power disturbance condition, the LEDA of operating point P_1 (represented as $\Omega_V(\boldsymbol{x}_{\mathbf{e1}})$) can be constructed. If $V(\boldsymbol{x}_{\mathbf{e0}}\text{-}\boldsymbol{x}_{\mathbf{e1}})$ holds the condition (19). It means the operating point $\boldsymbol{x}_{\mathbf{e0}} \in \Omega_V(\boldsymbol{x}_{\mathbf{e1}})$. So, the key step is to obtain the PFR of P_0 according to the condition (19).

From the characteristic of Lyapunov function $V(\boldsymbol{x})$, the following conclusion can be derived: 1) If the system power $P_0 = P_1$ (which means $\boldsymbol{x}_{\mathbf{e0}} = \boldsymbol{x}_{\mathbf{e1}}$), $V(\boldsymbol{x}_{\mathbf{e0}}\text{-}\boldsymbol{x}_{\mathbf{e1}}) = 0$; 2) the greater the deviation of P_1 from P_0, the larger value of $V(\boldsymbol{x}_{\mathbf{e0}}\text{-}\boldsymbol{x}_{\mathbf{e1}})$ will be. It can be deduced that when $V(\boldsymbol{x}_{\mathbf{e0}}\text{-}\boldsymbol{x}_{\mathbf{e1}}) = 1$ holds, the upper boundary of P_1 can be calculated, denoted as $P_{1\text{max}}$. Then, the largest feasible power disturbance $\triangle P_{\text{max}}$ at operating point P_0 is equal to $P_{1\text{max}} - P_0$. Therefore, the feasible region of P_0 is $\{0, -P_{\text{max}}\}$. To satisfy the largest power limit of the MCdc system, P_1 needs to be less than or equal to P_{neq}.

Algorithm: Construct the PFR Ω_{P}.

Input: The equilibrium point information of predisturbance (P_0), circuit parameters (L_{f}, C_{f}, L_{c}, R_{c}, and C_{Lf}), control parameters (k_{pi}, k_{ii}, k_{pv},k_{iv} and k_{d}), output voltage (V_0), rated power (P_{neq}), and threshold value $P_{\text{err}} = 0.1$ MW.
Initialization: $a = P_{\text{neq}}$, $b = P_0$.
While |a - b| $> P_{\text{err}}$
1) Set $P_1 = (\text{a} + \text{b})/2$. With the TS fuzzy model, an optimized Lyapunov function $V(\boldsymbol{x}_{\mathbf{e1}})$ of $\boldsymbol{x}_{\mathbf{e1}}$ can be constructed.
2) Calculate $e = V(\boldsymbol{x}_{\mathbf{e0}}\text{-}\boldsymbol{x}_{\mathbf{e1}})$
If $e < 1$ (Which indicates $\boldsymbol{x}_{\mathbf{e0}} \in \Omega_V(\boldsymbol{x}_{\mathbf{e1}})$)
Set $b = P_1$;
else if $e > 1$ (Which indicates $\boldsymbol{x}_{\mathbf{e0}} \notin \Omega_V(\boldsymbol{x}_{\mathbf{e1}})$)
Set $a = P_1$;
else
$a = b$;
End
End
3) Let $P_{1\text{max}} = P_1$;
Output: The PFR Ω_{P} represented by (20).

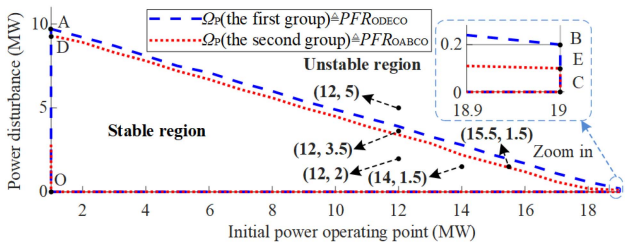

Fig. 9. Power feasible regions for the first and second group control parameters.

A PFR construction algorithm is proposed in this article, which is capable of inscribing the PFR of the ESC and its MCdc system.

With the help of the proposed algorithm, the PFRs $\text{PFR}_{\text{ODECO}}$ and $\text{PFR}_{\text{OABCO}}$ are inscribed for the first and second group control parameters, respectively, as shown in Fig. 9. Obviously, the transient stability of the MCdc system and its ESC model can be maintained if the power disturbance is within the PFR.

V. Theoretical Analysis and Experimental Verification

In this section, the influence of the control parameters on the PFR will be discussed.

A. Analysis of the Influence of K_{pi} on ΩP

The effect of the current proportional gain k_{pi} on the PFR Ω_{P} will be discussed in this subsection. In Fig. 10, $\text{PFR}_{\text{ODECO}}$,

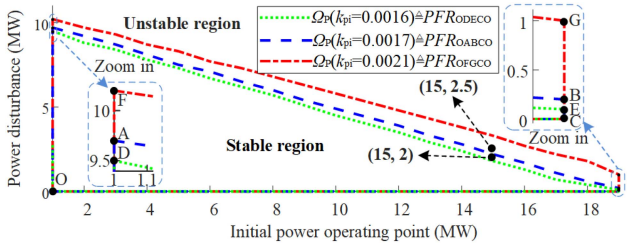

Fig. 10. Power feasible regions Ω_{P} with different proportional gain k_{pi}.

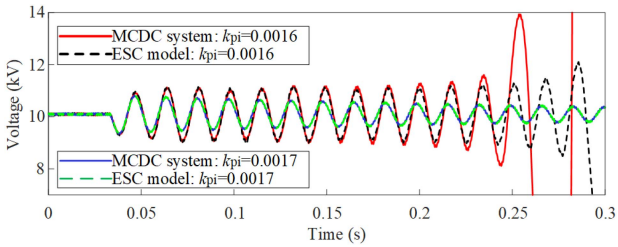

Fig. 11. Experimental results of CPL step from 15 to 17 MW.

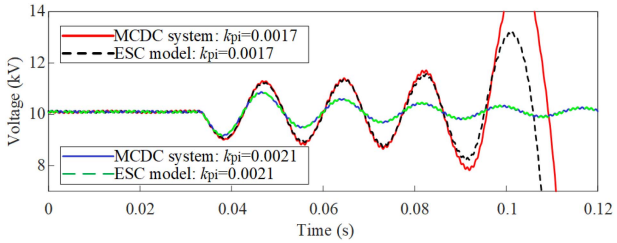

Fig. 12. Experimental results of CPL step from 15 to 17.5 MW.

$\mathrm{PFR}_{\mathrm{OABCO}}$, and $\mathrm{PFR}_{\mathrm{OFGCO}}$ are the PFRs for the current proportional gains of 0.0016, 0.0017, and 0.0021, respectively. From Fig. 10, it can be seen that increasing the current proportional gain will enlarge the PFR.

The point (15, 2 MW) is located outside the PFR $\mathrm{PFR}_{\mathrm{ODECO}}$ in Fig. 10. This indicates that the MCdc system and its ESC will lose the transient stability of the dc bus voltage. The instability experimental results for this theoretical analysis are provided by Fig. 11. Conversely, the dc bus voltage with a current proportional gain of 0.0017 is transiently stable after the same CPL disturbance. With the experimental results shown in Fig. 12, the conclusion that the transient stability of the MCdc system can be enhanced by increasing the current proportional gain is further verified.

B. Analysis of the Influence of K_{ii} on Ω_P

The PFRs for current integral gains of 0.1137, 0.1263, and 0.1390 are $\mathrm{PFR}_{\mathrm{OABCO}}$, $\mathrm{PFR}_{\mathrm{OABCO}}$, and $\mathrm{PFR}_{\mathrm{OAdcO}}$, respectively, as detailed in Fig. 12. Compared with the current proportional gain, increasing the current integral gain has a slight effect on the PFR Ω_{P}.

Based on the PFR $\mathrm{PFR}_{\mathrm{OABCO}}$ in Fig. 13, it can be known that their largest feasible disturbance power is both 3.1 MW at the 13-MW initial operating point. The experimental validation

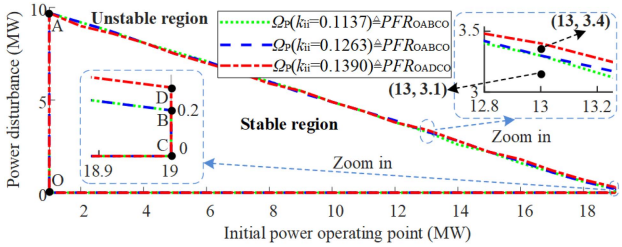

Fig. 13. PFR Ω_{P} with different integral gain k_{ii}.

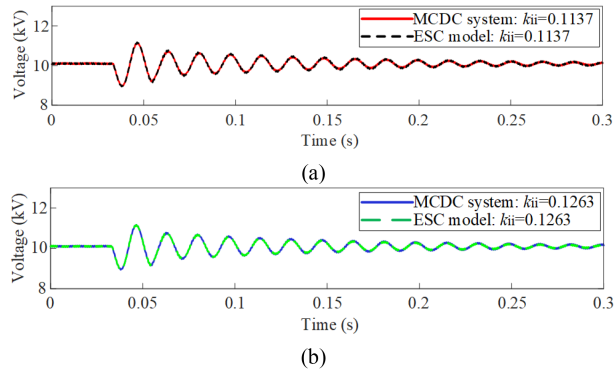

Fig. 14. Experimental results of CPL step from 13 to 16.1 MW: (a) $k_{\mathrm{ii}} = 0.1137$. (b) $k_{\mathrm{ii}} = 0.1263$.

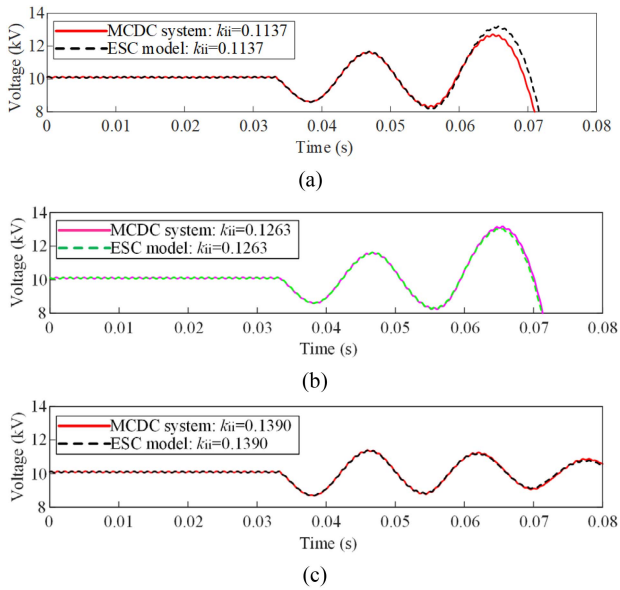

Fig. 15. Experimental results of CPL step from 13 to 16.4 MW: (a) $k_{\mathrm{ii}} = 0.1137$. (b) $k_{\mathrm{ii}} = 0.1263$. (c) $k_{\mathrm{ii}} = 0.1390$.

results are shown in Figs. 14 and 15, respectively. As can be seen in Fig. 14, their dc bus voltage can be stabilized after the CPL step from 13 to 16.1 WM. In addition, their dc bus voltage stability is simultaneously both lost after the 3.4-MW disturbance, as detailed in Fig. 15. It is worth noting that after the same 3.4-MW disturbance, the dc bus voltage with a current integral gain of 0.1390 is transiently stable. The main reason for this result is that the PFR has been effectively expanded, as shown in Fig. 13.

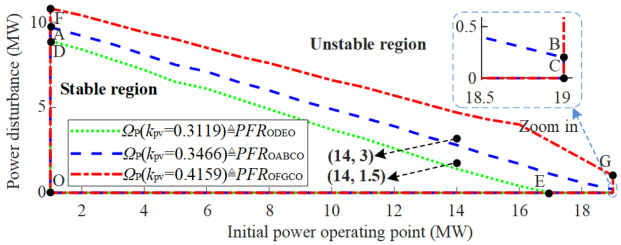

Fig. 16. Power feasible region Ω_P with different proportional gain k_{pv}.

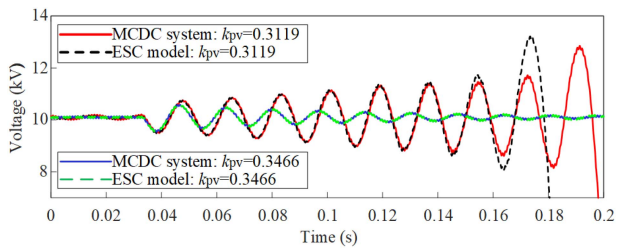

Fig. 17. Experimental results of CPL step from 14 to 15.5 MW.

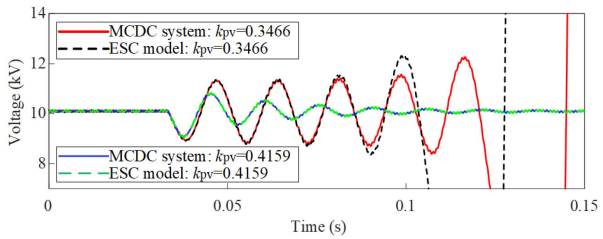

Fig. 18. Experimental results of CPL step from 14 to 17 MW.

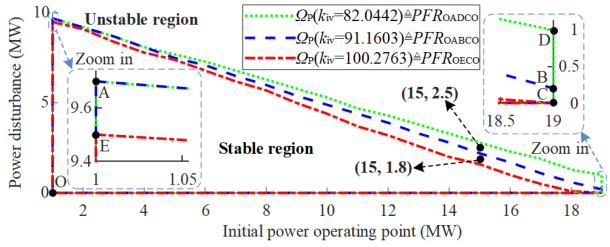

Fig. 19. Power feasible region Ω_P with different integral gain k_{iv}.

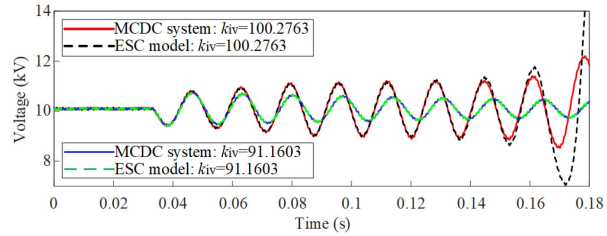

Fig. 20. Experimental results of CPL step from 15 to 16.8 MW.

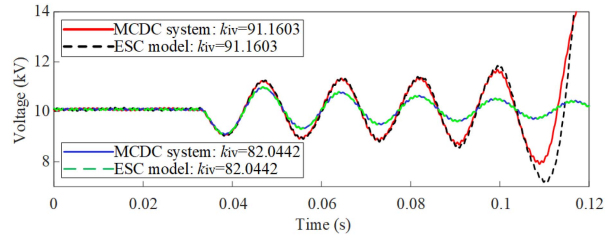

Fig. 21. Experimental results of CPL step from 15 to 17.5 MW.

C. Analysis of the Influence of K_{pv} on Ω_P

The change of voltage proportional gain will affect the PFR Ω_P, as detailed in this section. As can be seen in Fig. 16, with the increase of the voltage proportional gain, the PFR Ω_P will be enlarged. For example, the point (14, 1.5 MW) is located within the PFR PFR_{OABCO}, but outside the PFR PFR_{ODEO}. This means that after the CPL step from 14 to 15.5 MW, the dc bus voltage with a voltage proportional gain of 0.3119 will be transiently destabilized. On the contrary, the transient stability of dc bus voltage can be guaranteed if the voltage proportional gain is selected as 0.3466. Experimental verifications have been provided, as shown in Fig. 17. Based on the experimental results shown in Fig. 18, it is further verified that the transient stability of the dc bus voltage can be improved by increasing the voltage proportional gain. In addition, when the voltage proportional gain is set to 0.3119, it can be seen from Fig. 16 that the PFR at the initial operating point of 17 MW (also including 18 and 19 MW) is 0 MW. This means that these initial operating points will be small signal unstable.

D. Analysis of the Influence of K_{iv} on Ω_P

This subsection will focus on the influence of the variation of the voltage integral gain on the PFR Ω_P. As shown in Fig. 19, the PFRs for voltage integral gains of 82.0442, 91.1603, and 100.2763 are PFR_{OADCO}, PFR_{OABCO}. and PFR_{OECO}, respectively. It can be seen that the PFR will shrink with the increase of voltage integral gain within a certain range.

For the two experimental results of transient stability and instability in Fig. 20, their theoretical predictions have been given in Fig. 19. That is, the point (15, 1.8 MW) lies inside the PFR PFR_{OABCO}, but outside the PFR PFR_{OECO}. Based on the experimental results shown in Fig. 21, it is further verified that the transient stability of the dc bus voltage can be improved by decreasing the voltage integral gain.

E. Analysis of the Influence of K_d on Ω_P

When the droop coefficient is selected as 0.0067, 0.0767, and 0.1467, the corresponding PFR Ω_P are PFR_{OABCO}, PFR_{ODECO}, and PFR_{OFGCO}, respectively, as shown in Fig. 22. The results show that the larger the droop coefficient is, the larger the associated PFR will be.

The experimental results of the above feasible region analysis are shown in Figs. 23 and 24, respectively. As can be seen from Fig. 22, the point (15, 2.4MW) is not within the feasible region PFR_{OABCO}. Therefore, the transient stability will be lost in this case. This conclusion is proved by the instability experimental results in Fig. 23. However, as the droop coefficient increases

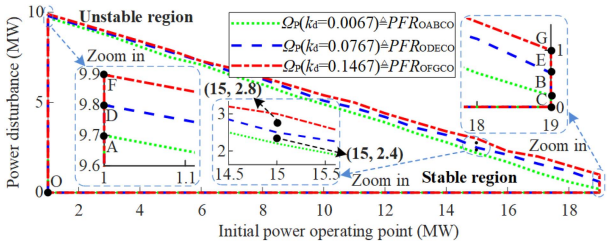

Fig. 22. Power feasible region Ω_{P} with different droop coefficient k_{d}.

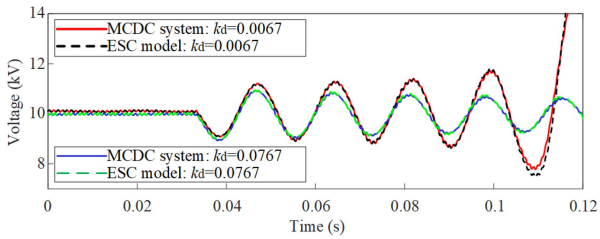

Fig. 23. Experimental results of CPL step from 15 to 17.4 MW.

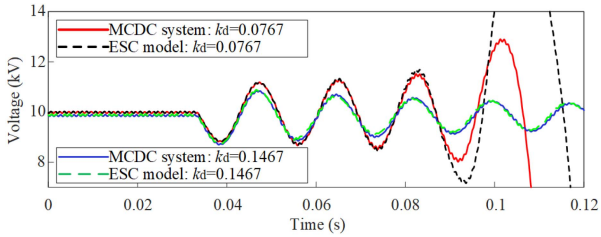

Fig. 24. Experimental results of CPL step from 15 to 17.8 MW.

from 0.0067 to 0.0767, the point (15, 2.4MW) will be transient stable, as shown in Fig. 22. The corresponding time domain verification results are provided in Fig. 23. With the time domain results in Fig. 24, the conclusion of Fig. 22 that the transient stability can be improved by increasing the droop coefficient is further verified.

As mentioned above, the control parameters have a significant impact on the transient stability of the MCdc system. To ensure the transient stability of the MCdc system, appropriate control parameters are very necessary. Moreover, the transient stability information contained in the PFR is very intuitive, rich, and practical. So, the PFR can be used as a new tool, which can provide theoretical guidance for the design of control parameters.

VI. Conclusion

In this article, based on the proposed system-level analysis method, the transient stability problem of droop-based MCdc system caused by large power disturbances is systematically investigated. From the perspective of reduced-order nonlinear mathematical modeling, the ESC model of the MCdc system is established by the proposed state-variable equivalent transformation method. On the basis, the LEDA is constructed by the TS fuzzy model of the ESC. Moreover, the PFR is depicted from the point of view of ensuring the transient stability of the MCdc system under large power disturbances. The main conclusions can be drawn as follows.

1) With this state-variable equivalent transformation method, an MCdc system containing $5*n+1$ state-variables can be modeled as an ESC model represented by six state-variables. Specifically, for the current control state-variable $\int(I_{\mathrm{r}}\text{-}I)\mathrm{d}t$ of the ESC model, which is equal to the sum of all current control state-variables $\int(I_{\mathrm{r}y}\text{-}I_y)\mathrm{d}t$ in the MCdc system. And for each voltage control state-variable $\int(V_{\mathrm{ref}y}\text{-}I_{\mathrm{c}y}k_{\mathrm{d}y}\text{-}V_{Cfy})\mathrm{d}t$ in the MCdc system, they are consistent with the voltage control state-variable $\int(V_{\mathrm{ref}}\text{-}I_{\mathrm{c}}k_{\mathrm{d}}\text{-}V_{Cf})\mathrm{d}t$ of the ESC model. The consistent transient stability or instability of the MCdc system and its ESC model has been verified by numerous experimental results.
2) The TS fuzzy model of the ESC is developed in this article, which can be used to construct the LEDA. As long as the predisturbance operating point lies within the LEDA of the postdisturbance operating point, then both the MCdc system and its ESC model will be transient stable. Conversely, they will both become transient unstable.
3) Based on the LEDA obtained from the TS fuzzy model, the PFR is inscribed by the proposed construction algorithm. If the large power disturbance is within the PFR, the transient stability of both the MCdc system and its ESC model can be guaranteed. On the contrary, their transient stability will be lost simultaneously. With the increase of voltage proportional gain, current proportional gain, and droop coefficient or the decrease of voltage integral gain, the PFR will be enlarged. However, the PFR will change slightly with the variation of the current integral gain.

It should be noted that this state-variable equivalent transformation method still has some limitations. For instance, the necessary condition of this method is the consistent dynamic characteristics of each source converter. However, for hybrid energy storage systems, the dynamic characteristics of different source converters are quite different. In this situation, how to establish the ESC model will be the future research work. In addition, the interaction mechanism between different load converters is difficult to be revealed by this method. In the future, the transient stability of MCdc system considering the interaction of different load converters will be discussed.

Appendix A

The switching models of the MCdc system and its ESC model shown in Fig. 1 are built in the RT-BOX hardware-in-the-loop experimental platform for theoretical analysis and experimental verification, respectively. The circuit parameters and control parameters of the MCdc system (including two converters) are shown in Tables II and III, respectively.

TABLE II
CIRCUIT PARAMETERS OF THE MCDC SYSTEM

Equipment name	Parameter	Value
1st converter	Rated output power P_{n1}/MW	15
	Filter inductor L_{f1}/mH	26.7
	Filter capacitor C_{f1}/mF	0.09375
	Switching frequency f_{s1}/kHz	1
	Cable inductor mH	0.25
	Cable resistor Ω	0.1179
2nd converter	Rated output power P_{n2}/MW	5
	Filter inductor L_{f2}/mH	80
	Filter capacitor C_{f2}/mF	0.03125
	Switching frequency f_{s2}/kHz	1
	Cable inductor mH	0.752
	Cable resistor Ω	0.3536
CPL	Rated output power P_{eq}/MW	20
	Input filter capacitor C_{Lfeq}/mF	1

TABLE III
CONTROL PARAMETERS OF THE MCDC SYSTEM

	Parameter	Value	Parameter	Value
Group 1	k_{pi1}	0.0022	k_{pi2}	0.0068
	k_{ii1}	0.1685	k_{ii2}	0.5054
	k_{pv1}	0.2534	k_{pv2}	0.0845
	k_{iv1}	68.370	k_{iv2}	22.790
	k_{d1}	0.0089	k_{d2}	0.0268
Group 2	k_{pi1}	0.0023	k_{pi2}	0.0070
	k_{ii1}	0.1685	k_{ii2}	0.5054
	k_{pv1}	0.2599	k_{pv2}	0.0866
	k_{iv1}	68.370	k_{iv2}	22.790
	k_{d1}	0.0089	k_{d2}	0.0268

As shown in Fig. 25, it can be seen that the phase margins of the three closed-loop transfer functions are all positive. This means that all three operating points (i.e., 12, 14, and 15.5 MW) mentioned above are small signal stable at the first group control parameters. Similarly, the small signal stability analysis results for the second group control parameters can also be obtained, as shown in Fig. 26.

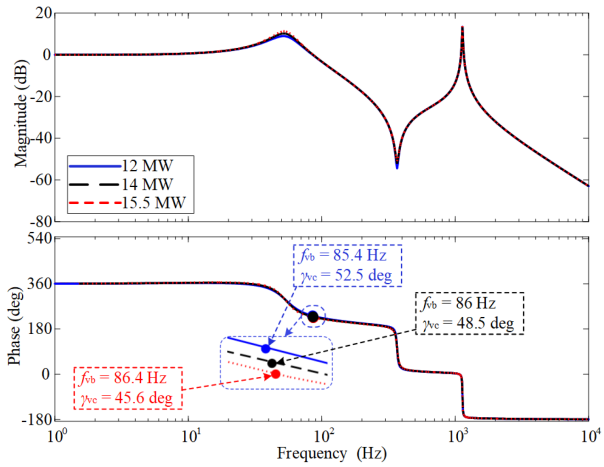

Fig. 25. Bode diagram for the first group control parameters.

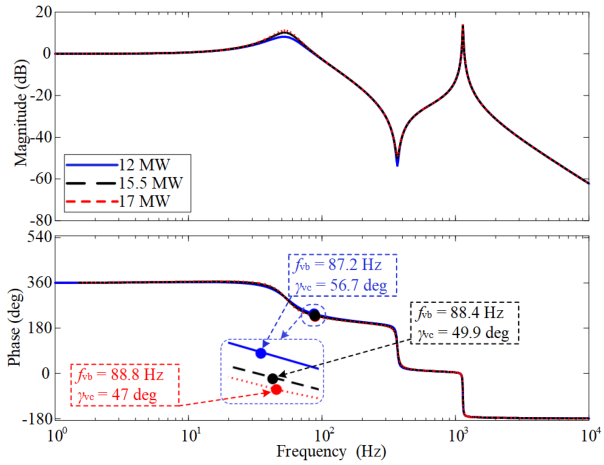

Fig. 26. Bode diagram for the second group control parameters.

APPENDIX B

A. Equivalent Transformation of Voltage Control State-Variables

According to the design guidelines recommended by [31], the relationship between the voltage control parameters of each converter can be written as (B.1). Similarly, the relationship between the current control parameters of each converter can be expressed as (B.2)

$$\begin{cases} \dfrac{k_{pvy}}{k_{pv(y+1)}} = \dfrac{h_y}{h_{(y+1)}} \\ \dfrac{k_{ivy}}{k_{iv(y+1)}} = \dfrac{h_y}{h_{(y+1)}} \end{cases} \tag{B.1}$$

$$\begin{cases} \dfrac{k_{piy}}{L_{fy}} = \dfrac{k_{pi(y+1)}}{L_{f(y+1)}} \\ \dfrac{k_{iiy}}{L_{fy}} = \dfrac{k_{ii(y+1)}}{L_{f(y+1)}}. \end{cases} \tag{B.2}$$

Hence, the equivalent droop coefficient k_d can be given by

$$\frac{1}{k_d} = \sum_{y=1}^{n} \left(\frac{1}{k_{dy}} \right). \tag{B.3}$$

B. Equivalent Transformation of Current Control State-Variables

Obviously, (9) can be reconstructed as follows:

$$\begin{cases} \dfrac{D_{eq} \cdot V_s}{L_f} = \sum_{y=1}^{n} \left(\dfrac{D_y \cdot V_{sy}}{L_{fy}} \right) \\ \dfrac{V_{Cf}}{L_f} = \sum_{y=1}^{n} \left(\dfrac{V_{Cfy}}{L_{fy}} \right). \end{cases} \tag{B.4}$$

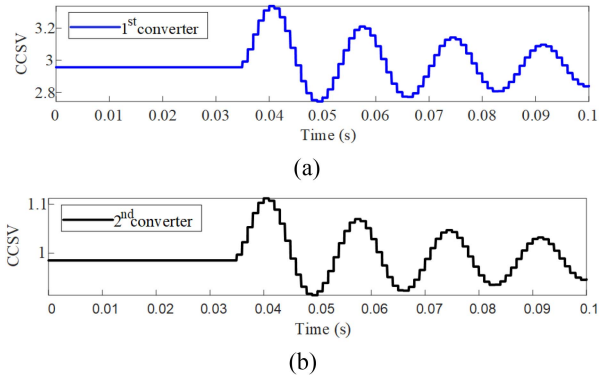

Fig. 27. Waveforms of current control state-variables under Case 1. (a) 1st converter. (b) 2nd converter.

Since all input voltage sources are identical to each other in this article, i.e., $V_{\rm s} = V_{{\rm s}y}$, then (B.4) can be simplified as follows:

$$\begin{cases} \dfrac{D_{\rm eq}}{L_{\rm f}} = \sum_{y=1}^{n} \left(\dfrac{D_y}{L_{{\rm f}y}} \right) \\ \dfrac{1}{L_{\rm f}} \approx \sum_{y=1}^{n} \left(\dfrac{1}{L_{{\rm f}y}} \right). \end{cases} \tag{B.5}$$

The analytical equation between the output filter inductor $L_{{\rm f}y}$ of each converter and the output filter inductor $L_{\rm f}$ of the ESC model can be established, as shown in (B.5). Since all output filter capacitors $C_{{\rm f}y}$ are connected in parallel, then the equivalent output filter capacitor $C_{\rm f}$ can be given by

$$C_{\rm f} \approx \sum_{y=1}^{n} C_{{\rm f}y} \tag{B.6}$$

where $C_{\rm f}$ is the output filter capacitor of the ESC model. Considering the current control loop, (B.5) can be reconstructed as follows:

$$\begin{aligned} &\frac{k_{\rm pi}(I_{\rm r}-I)+k_{\rm ii}\int (I_{\rm r}-I)dt}{L_{\rm f}} \\ &= \sum_{y=1}^{n} \left(\frac{k_{{\rm pi}y}(I_{{\rm r}y}-I_y)+k_{{\rm ii}y}\int (I_{{\rm r}y}-I_y)dt}{L_{{\rm f}y}} \right) \end{aligned} \tag{B.7}$$

where $k_{{\rm pi}y}$ and $k_{{\rm ii}y}$ are the proportional and integral gains of the current controller $G_{{\rm cc}y}(s)$ of the yth converter, respectively, $k_{\rm pi}$ and $k_{\rm ii}$ are the proportional and integral gains of the current controller $G_{\rm cc}(s)$ of the ESC model, respectively.

C. Verification of Equivalent Transformation of State-Variables

Due to the length limitation of this article, the time domain results of the state-variables of Case1 are given. From the current control state-variable (CCSV) waveforms shown in Fig. 27, it can be found that the state-variable $\int(I_{\rm r1} - I_1){\rm d}t$ is three times larger than the current control state-variable $\int(I_{\rm r2} - I_2){\rm d}t$. This is opposite to the ratio of the current integral gain between the two converters. More importantly, the state-variable $\int(I_{\rm r} - I){\rm d}t$ of the ESC model is almost the same as the sum of the state-variables $\int(I_{\rm r1} - I_1){\rm d}t$ and $\int(I_{\rm r2} - I_2){\rm d}t$, as shown in Fig. 28.

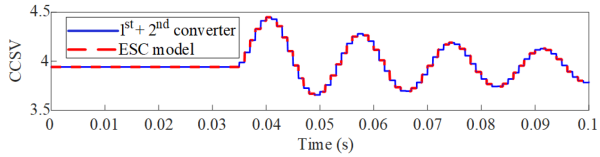

Fig. 28. Waveforms of current control state-variables (1st converter, 2nd converter, and the ESC model) under Case 1.

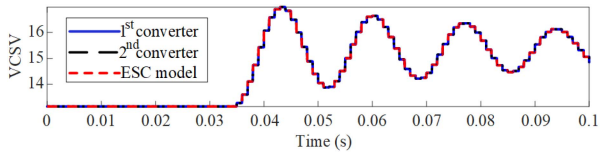

Fig. 29. Waveforms of voltage control state-variables (1st converter, 2nd converter, and the ESC model) under Case 1.

Similarly, in Fig. 29, the voltage control state-variable (VCSV) waveforms of the two converters and the ESC model are also almost consistent.

Appendix C

The existing methods used to generate Lyapunov functions include the Lyapunov direct method [27], mixed potential theory [20], [21], TS fuzzy model method [18], and so on. Considering the advantages and disadvantages of the above methods, the TS fuzzy model method is preferred in this article. This is mainly because it can consider both the circuit dynamics and control dynamics of the system. The methodological steps for constructing the Lyapunov function and inscribing the estimated domain of attraction by the TS fuzzy model approach are detailed as follows, as in [2].

Step 1: The nonlinear system can be written in the form of $\dot{\boldsymbol{x}} = \boldsymbol{A}(\boldsymbol{x})\boldsymbol{x}$, where $\boldsymbol{A}(\boldsymbol{x})$ is a nonlinear matrix function containing state-variables and $\boldsymbol{x}$ is the state-variable column matrix.

Step 2: Select a small region $\boldsymbol{\Omega}$ around the equilibrium point and denote its boundary as $\partial\boldsymbol{\Omega}$. And, the maximum value $x_{i\max}$ and the minimum value $x_{i\min}$ of the ith nonlinear term in $\boldsymbol{A}(\boldsymbol{x})$ with this region $\boldsymbol{\Omega}$ can be obtained. Then, the matrices $\boldsymbol{A}_{i\max}$ and $\boldsymbol{A}_{i\min}$ can be obtained as the ith nonlinear term in $\boldsymbol{A}(\boldsymbol{x})$ is replaced by the minimum value $x_{i\min}$ and the maximum value $x_{i\max}$, respectively.

Step 3: If the linear matrix inequality (C.1) is feasible, then the system is asymptotically stable within the region $\Omega_{\rm c} = \{\boldsymbol{x}\in\mathbf{R}^N | \ V(\boldsymbol{x})\leq\min(V(\partial\Omega))\}$, where $V(\boldsymbol{x}) = \boldsymbol{x}^{\mathbf{T}}\boldsymbol{M}\boldsymbol{x}$.

$$\begin{cases} M = M^T > 0 \\ A_{i\max}^T M + M A_{i\max} < 0 \quad i = 1, 2, \ldots, m \\ A_{i\min}^T M + M A_{i\min} < 0 \quad i = 1, 2, \ldots, m \end{cases} \tag{C.1}$$

where M is the symmetric matrix, N and m are the number of state-variables and nonlinear terms.

Step 4: Keep increasing $\boldsymbol{\Omega}$ until the linear matrix inequality (C.1) is infeasible. At this point, $\boldsymbol{\Omega}_{\rm c}$ is the LEDA of the system. (C.2) and (C.3) shown at the top of the next page.

$$\begin{cases} C_{\rm f}\frac{dV}{dt} = I - I_{\rm c} \\ L_{\rm f}\frac{dI}{dt} = D_{\rm eq}\cdot V_{\rm s} - V_{C\rm f} \\ L_{\rm c}\frac{dI_{\rm c}}{dt} = V_{C\rm f} - I_{\rm c}\cdot R_{\rm c} - V \end{cases} \quad \begin{cases} C_{\rm cpl}\frac{dV}{dt} = I_{\rm c} - \frac{P_{\rm cpl}}{V} \\ D_{\rm eq} = \ k_{\rm ip}k_{\rm pv}\left(V_{\rm ref} - I_{\rm c}\cdot k_{\rm d} - V_{C\rm f}\right) \\ \qquad +k_{\rm ip}\left\{k_{\rm iv}\int\left(V_{\rm ref} - I_{\rm c}\cdot k_{\rm d} - V_{C\rm f}\right)dt - I\right\} + k_{\rm ii}\int\left(I_{\rm r} - I\right)dt \end{cases} \tag{C.2}$$

$$\begin{bmatrix} \dot{x}_1 \\ \dot{x}_2 \\ \dot{x}_3 \\ \dot{x}_4 \\ \dot{x}_5 \\ \dot{x}_6 \end{bmatrix} = \begin{bmatrix} 0 & -k_{\rm ii} & k_{\rm ii} & -k_{\rm ii}k_{\rm pv} & -k_{\rm ii}k_{\rm pv}k_{\rm d} & 0 \\ \frac{V_{\rm s}}{L_{\rm f}} & -\frac{V_{\rm s}k_{\rm ip}}{L_{\rm f}} & \frac{V_{\rm s}k_{\rm ip}}{L_{\rm f}} & -\frac{V_{\rm s}k_{\rm ip}k_{\rm pv}+1}{L_{\rm f}} & -\frac{k_{\rm d}V_{\rm s}k_{\rm ip}k_{\rm pv}}{L_{\rm f}} & 0 \\ 0 & 0 & 0 & -k_{\rm iv} & -k_{\rm iv}k_{\rm d} & 0 \\ 0 & \frac{1}{C_{\rm f}} & 0 & 0 & -\frac{1}{C_{\rm f}} & 0 \\ 0 & 0 & 0 & \frac{1}{L_{\rm c}} & 0 & -\frac{1}{L_{\rm c}} \\ 0 & 0 & 0 & 0 & \frac{1}{C_{\rm cpl}} & \frac{P_{\rm cpl}}{C_{\rm cpl}\cdot V_0\cdot(x_6+V_0)} \end{bmatrix} \begin{bmatrix} x_1 \\ x_2 \\ x_3 \\ x_4 \\ x_5 \\ x_6 \end{bmatrix}. \tag{C.3}$$

REFERENCES

[1] N. Hatziargyriou et al., "Definition and classification of power system stability–revisited & extended," *IEEE Trans. Power Syst.*, vol. 36, no. 4, pp. 3271–3281, Jul. 2021.

[2] D. Marx, P. Magne, B. Nahid-Mobarakeh, S. Pierfederici, and B. Davat, "Large signal stability analysis tools in DC power systems with constant power loads and variable power loads—A review," *IEEE Trans. Power Electron.*, vol. 27, no. 4, pp. 1773–1787, Apr. 2012.

[3] M. Kabalan, P. Singh, and D. Niebur, "Large signal Lyapunov-based stability studies in microgrids: A review," *IEEE Trans. Smart Grid*, vol. 8, no. 5, pp. 2287–2295, Sep. 2017.

[4] W. Du, Q. Fu, and H. F. Wang, "Small-signal stability of a DC network planned for electric vehicle charging," *IEEE Trans. Smart Grid*, vol. 11, no. 5, pp. 3748–3762, Sep. 2020.

[5] R. Han, H. Wang, Z. Jin, L. Meng, and J. M. Guerrero, "Compromised controller design for current sharing and voltage regulation in DC microgrid," *IEEE Trans. Power Electron.*, vol. 34, no. 8, pp. 8045–8061, Aug. 2019.

[6] M. Leng, G. Zhou, H. Li, G. Xu, F. Blaabjerg, and T. Dragičević, "Impedance-based stability evaluation for multibus DC microgrid without constraints on subsystems," *IEEE Trans. Power Electron.*, vol. 37, no. 1, pp. 932–943, Jan. 2022.

[7] P. Li et al., "Reduced-order modeling and comparative dynamic analysis of DC voltage control in DC microgrids under different droop methods," *IEEE Trans. Energy Convers.*, vol. 36, no. 4, pp. 3317–3333, Dec. 2021.

[8] L. Zhou et al., "Virtual positive-damping reshaped impedance stability control method for the offshore MVDC system," *IEEE Trans. Power Electron.*, vol. 34, no. 5, pp. 4951–4966, May 2019.

[9] Y. Li et al., "Modeling and damping control of modular multilevel converter based DC grid," *IEEE Trans. Power Syst.*, vol. 33, no. 1, pp. 723–735, Jan. 2018.

[10] B. He, W. Chen, X. Ruan, X. Zhang, Z. Zou, and W. Cao, "A generic small-signal stability criterion of DC distribution power system: Bus node impedance criterion (BNIC)," *IEEE Trans. Power Electron.*, vol. 37, no. 5, pp. 6116–6131, May 2022.

[11] B. He, W. Chen, X. Li, L. Shu, and X. Ruan, "A power adaptive impedance reshaping strategy for cascaded DC system with buck-type constant power load," *IEEE Trans. Power Electron.*, vol. 37, no. 8, pp. 8909–8920, Aug. 2022.

[12] R. Shen and H. S. -H. Chung, "On the use of nonlinear inductor to enhance the stability of DC distribution networks," *IEEE Trans. Power Electron.*, vol. 37, no. 7, pp. 8582–8595, Jul. 2022.

[13] C. Zhang, X. Wang, P. Lin, P. X. Liu, Y. Yan, and J. Yang, "Finite-time feedforward decoupling and precise decentralized control for DC microgrids towards large-signal stability," *IEEE Trans. Smart Grid*, vol. 11, no. 1, pp. 391–402, Jan. 2020.

[14] L. Xu et al., "A review of DC shipboard microgrids—Part I: Power architectures, energy storage, and power converters," *IEEE Trans. Power Electron.*, vol. 37, no. 5, pp. 5155–5172, May 2022.

[15] L. Xu et al., "A review of DC shipboard microgrids—Part II: Control architectures, stability analysis, and protection schemes," *IEEE Trans. Power Electron.*, vol. 37, no. 4, pp. 4105–4120, Apr. 2022.

[16] M. H. Roos, P. H. Nguyen, J. Morren, and J. G. Slootweg, "Stability analysis of microgrid islanding transients based on interconnected dissipative subsystems," *IEEE Trans. Smart Grid*, vol. 12, no. 6, pp. 4655–4667, Nov. 2021.

[17] M. N. Hussain, R. Mishra, and V. Agarwal, "A frequency-dependent virtual impedance for voltage-regulating converters feeding constant power loads in a DC microgrid," *IEEE Trans. Ind. Appl.*, vol. 54, no. 6, pp. 5630–5639, Nov./Dec. 2018.

[18] H. J. Kim, S. W. Kang, G. S. Seo, P. Jang, and B. H. Cho, "Large-signal stability analysis of DC power system with shunt active damper," *IEEE Trans. Ind. Electron.*, vol. 63, no. 10, pp. 6270–6280, Oct. 2016.

[19] Y. Gui, R. Han, J. M. Guerrero, J. C. Vasquez, B. Wei, and W. Kim, "Large-signal stability improvement of DC-DC converters in DC microgrid," *IEEE Trans. Energy Convers.*, vol. 36, no. 3, pp. 2534–2544, Sep. 2021.

[20] M. Huang, H. Ji, J. Sun, L. Wei, and X. Zha, "Bifurcation-based stability analysis of photovoltaic-battery hybrid power system," *IEEE J. Emerg. Sel. Topics Power Electron.*, vol. 5, no. 3, pp. 1055–1067, Sep. 2017.

[21] J. Jiang et al., "A conservatism-free large signal stability analysis method for DC microgrid based on mixed potential theory," *IEEE Trans. Power Electron.*, vol. 34, no. 11, pp. 11342–11351, Nov. 2019.

[22] Y. Xia, W. Wei, T. Long, F. Blaabjerg, and P. Wang, "New analysis framework for transient stability evaluation of DC microgrids," *IEEE Trans. Smart Grid*, vol. 11, no. 4, pp. 2794–2804, Jul. 2020.

[23] S. Liu, X. Li, M. Xia, Q. Qin, and X. Liu, "Takagi-sugeno multimodeling-based large signal stability analysis of DC microgrid clusters," *IEEE Trans. Power Electron.*, vol. 36, no. 11, pp. 12670–12684, Nov. 2021.

[24] A. P. N. Tahim, D. J. Pagano, E. Lenz, and V. Stramosk, "Modeling and stability analysis of islanded DC microgrids under droop control," *IEEE Trans. Power Electron.*, vol. 30, no. 8, pp. 4597–4607, Aug. 2015.

[25] G. Sulligoi, D. Bosich, G. Giadrossi, L. Zhu, M. Cupelli, and A. Monti, "Multiconverter medium voltage DC power systems on ships: Constant-power loads instability solution using linearization via state feedback control," *IEEE Trans. Smart Grid*, vol. 5, no. 5, pp. 2543–2552, Sep. 2014.

[26] D. Bosich, G. Sulligoi, E. Mocanu, and M. Gibescu, "Medium voltage DC power systems on ships: An offline parameter estimation for tuning the controllers' linearizing function," *IEEE Trans. Energy Convers.*, vol. 32, no. 2, pp. 748–758, Jun. 2017.

[27] W. Xie, M. Han, W. Cao, J. M. Guerrero, and J. C. Vasquez, "System-level large-signal stability analysis of droop-controlled DC microgrids," *IEEE Trans. Power Electron.*, vol. 36, no. 4, pp. 4224–4236, Apr. 2021.

[28] W. Xie, M. Han, W. Cao, J. M. Guerrero, and J. C. Vasquez, "Virtual resistance tradeoff design for DCMG grid-forming converters considering static- and large-signal dynamic constraints," *IEEE Trans. Power Electron.*, vol. 36, no. 5, pp. 5582–5593, May 2021.

[29] B. A. Martinez-Treviño, A. E. Aroudi, A. Cid-Pastor, and L. Martinez-Salamero, "Nonlinear control for output voltage regulation of a boost converter with a constant power load," *IEEE Trans. Power Electron.*, vol. 34, no. 11, pp. 10381–10385, Nov. 2019.

[30] B. A. Martínez-Treviño, A. E. Aroudi, H. Valderrama-Blavi, A. Cid-Pastor, E. Vidal-Idiarte, and L. Martinez-Salamero, "PWM nonlinear control with load power estimation for output voltage regulation of a boost converter with constant power load," *IEEE Trans. Power Electron.*, vol. 36, no. 2, pp. 2143–2153, Feb. 2021.

[31] Q. Xu, Y. Yan, C. Zhang, T. Dragicevic, and F. Blaabjerg, "An offset-free composite model predictive control strategy for DC/DC buck converter feeding constant power loads," *IEEE Trans. Power Electron.*, vol. 35, no. 5, pp. 5331–5342, May 2020.

Xueshen Zhao (Student Member, IEEE) received the B.Sc. and M.Sc. degrees in electrical engineering from the Shandong University of Technology, Shandong, China, in 2016 and 2019, respectively. He is currently working toward the Ph.D. degree in electrical engineering with Tianjin University, Tianjin, China.

His research interests include modeling, stability analysis, and control of power electronics dominated power systems.

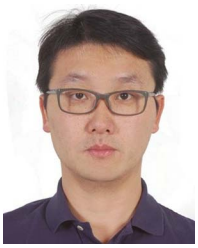

Li Guo (Member, IEEE) received the B.Sc. and the Ph.D. degree in electrical engineering from the South China University of Technology, Guangzhou, China, in 2002 and 2007, respectively.

He is currently a Full Professor with Tianjin University, Tianjin, China. His research interests include the optimal planning and design of microgrid, the coordinated operating strategy of microgrid, and the advanced energy management system.

Lin Zhu (Member, IEEE) received the B.Sc. and M.Sc. degrees from China Agriculture University, Beijing, China, in 2008 and 2010, respectively, and the Ph.D. degree from RWTH Aachen University, Aachen, Germany, in 2018, all in electrical engineering.

Since 2010, she has been a Research Associate with the Institute of Automation of Complex Power Systems, E.ON Energy Research Center, Aachen, Germany. Since 2019, she has been a Lecturer with the School of Electrical Engineering and Automation, Tianjin University, Tianjin, China. Her research interests include stability analysis, control and hardware in the loop simulation in dc, and hybrid ac/dc power systems.

Xialin Li (Member, IEEE) received the B.Sc. and Ph.D. degrees in electrical engineering from Tianjin University, Tianjin, China, in 2009 and 2014, respectively.

Since 2014, he has been a Lecturer with the School of Electrical Engineering and Automation, Tianjin University, Tianjin, China. In 2016, under the State Scholarship Fund, he was invited as a Visiting Professor to the Department of Electrical and Computer Engineering, University of Alberta, Edmonton, AB, Canada. His research interests include the modeling and control of power converters, distributed generation, hybrid ac/dc microgrid, and multiterminal dc grids.

Zhi Wang received the B.S. degree in electrical engineering, in 2020, from Tianjin University, Tianjin, China, where he is currently working toward the M.Sc. degree in electrical engineering.

His research interests include stability analysis and control in dc power system.

Chengshan Wang (Senior Member, IEEE) received the B.Sc., M.Sc., and Ph.D. degrees in electrical engineering from Tianjin University, Tianjin, China, in 1983, 1985 and 1991, respectively.

He became a Full Professor with Tianjin University, in 1996. He was a Visiting Scientist with Cornell University, Ithaca, NY, USA, from 1994 to 1996, and a Visiting Professor with Carnegie Mellon University, Pittsburgh, PA, USA, from 2001 to 2002. He is the Chief Scientist of the 973 project, "Research on the Key Issues of Distributed Generation Systems," from 2009 to 2013 that had Chinese power engineering scientists participating from eight leading institutions. His research interests include distribution system analysis and planning, distributed generation system and microgrid, and power system security analysis.

Dr. Wang was the recipient of the Fok Ying Tung Fund, Excellent Young Teacher Fund of Education Ministry and the National Science Fund for Distinguished Young Scholars.